Production of cascade hypernuclei via the (K^-, K^+) reaction within a quark-meson coupling model

R. Shyam[a,b], K. Tsushima[a], A.W. Thomas[a]

[a] *Centre for the Subatomic Structure of Matter (CSSM), School of Chemistry and Physics, University of Adelaide, SA 5005, Australia*
[b] *Saha Institute of Nuclear Physics, 1/AF Bidhan Nagar, Kolkata 700064, India*

Abstract

We study the production of bound hypernuclei ${}^{12}_{\Xi^-}$Be and ${}^{28}_{\Xi^-}$Mg via the (K^-, K^+) reaction on ^{12}C and ^{28}Si targets, respectively, within a covariant effective Lagrangian model, employing Ξ bound state spinors derived from the latest quark-meson coupling model as well as Dirac single particle wave functions. The $K^+\Xi^-$ production vertex is described by excitation, propagation and decay of Λ and Σ resonance states in the initial collision of a K^- meson with a target proton in the incident channel. The parameters of the resonance vertices are fixed by describing the available data on total and differential cross sections for the $p(K^-, K^+)\Xi^-$ reaction. We find that both the elementary and hypernuclear production cross sections are dominated by the contributions from the $\Lambda(1520)$ intermediate resonant state. The 0° differential cross sections for the formation of simple s-state Ξ^- particle-hole states peak at a beam momentum around 1.0 GeV/c, with a value in excess of 1 μb.

Keywords: Cascade hypernuclei, covariant model of (K^-, K^+) reaction, quark-meson coupling model cascade spinors.
PACS: 25.80.Nv, 24.85.+p, 13.75.Jz

1. Introduction

The study of the double strangeness (S) hypernuclei is of decisive importance for revealing the entire picture of strong interactions among octet baryons. The binding energies and widths of the Ξ hypernuclear states are expected to determine the strength of the ΞN and $\Xi N \to \Lambda\Lambda$ interactions, respectively. This basic information is key to testing the quark exchange aspect of the strong interaction because long range pion exchange plays essentially a very minor role in the $S = -2$ sector. Even though t-channel pion exchange between Ξ and nucleon does operate, its strength is quite weak because the $\pi\Xi\Xi$ coupling is smaller as compared to the πNN coupling [1]. This input is also vital for understanding the multi-strange hadronic or quark matter. Since strange quarks are negatively charged they are preferred in charge neutral dense matter. Thus these studies are of crucial value for investigating the role of strangeness in the

equation of state at high density, as probed in the cores of neutron stars [2, 3] and in high energy heavy ion collisions at relativistic heavy ion colliders (RHIC) at Brookhaven National laboratory [4], CERN [5] and FAIR facility at GSI [6].

The (K^-, K^+) reaction leads to the transfer of two units of both charge and strangeness to the target nucleus. Thus this reaction is one of the most promising ways of studying the $S = -2$ systems such as Ξ hypernuclei and a dibaryonic resonance (H), which is a near stable six-quark state with spin parity of 0^+ and isospin 0 [7, 8, 9]. Several ways have been discussed to approach these systems in the past [10, 11]. Many experimental groups have used the (K^-, K^+) reaction on nuclear targets to search for a H dibaryonic resonance [12, 13, 14, 15, 16].

As far as Ξ hypernuclei are concerned, there are some hints of their existence from emulsion events [17]. However, no Ξ bound state was unambiguously observed in the few experiments performed involving the (K^-, K^+) reaction on a ^{12}C target [13, 15] because of the limited statistics and detector resolution. However, in the near future experiments will be performed at the JPARC facility in Japan to observe the bound states of Ξ hypernuclei via the (K^-, K^+) reaction with the best energy resolution of a few MeV and with large statistics by using the newly constructed high-resolution spectrometers [18]. The first series of experiments will be performed on a ^{12}C target. These measurements are of great significance because convincing evidence for the Ξ single-particle bound states would yield vital information on Ξ single particle potential and the effective ΞN interaction. Already, the analysis of the scarce emulsion [19] and spectrometer data [13, 15] have led to Ξ-nuclear potentials with depths that differ by about 10 MeV from each other.

The (K^-, K^+) reaction implants a Ξ hyperon in the nucleus through the elementary process $p(K^-, K^+)\Xi^-$. The cross sections for the elementary reaction were measured in the 1960s and early 1970s using hydrogen bubble chambers [20, 21, 22, 23, 24, 25]. The total cross-section data from these measurements are tabulated in Ref. [26]. In a recent study [27], this reaction was investigated within a single-channel effective Lagrangian model where contributions were included from the s-channel [see, Fig. 1(a)] and u-channel diagrams which have as intermediate states Λ and Σ hyperons together with eight of their three- and four-star resonances with masses up to 2.0 GeV [$\Lambda(1405)$, $\Lambda(1520)$, $\Lambda(1670)$, $\Lambda(1810)$, $\Lambda(1890)$, $\Sigma(1385)$, $\Sigma(1670)$ and $\Sigma(1750)$, which are represented by Λ^* and Σ^* in Fig. 1a]. This reaction is a clean example of a process in which baryon exchange plays the dominant role and the t-channel meson exchanges are absent, as no meson with $S = +2$ is known to exist. An important observation of that study is that the total cross section of the $p(K^-, K^+)\Xi^-$ reaction is dominated by the contributions from the $\Lambda(1520)$ (with $L_{I2J} = D_{03}$) resonance intermediate state through both s- and u-channel terms. The region for beam momentum (p_{K^-}) below 2.0 GeV/c was shown to get most contributions from the s-channel graphs - the u-channel terms are dominant only in the region p_{K^-} > 2.5 GeV.

Almost all of the previous theoretical investigations of cascade hypernuclear production via (K^-, K^+) reaction on target nuclei [19, 28, 29, 30, 31] have used the framework of an impulse approximation where the hyperon production

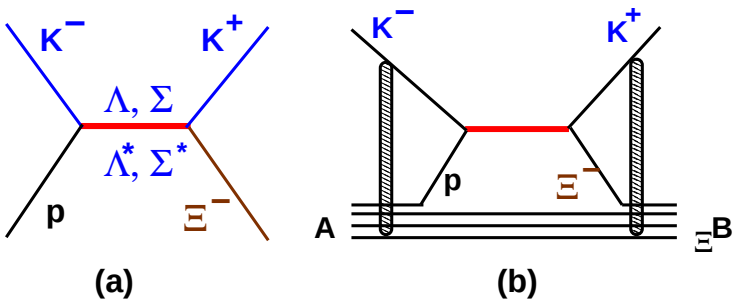

Figure 1: (color online) Graphical representation of our model to describe $p(K^-, K^+)\Xi^-$ (Fig. 1a) and $A(K^-, K^+)_{\Xi^-}$B reactions (Fig. 2b). In the latter case the shaded area depicts the optical model interactions in the incoming and outgoing channels.

dynamics is separated from that of the relative motion in the entrance and outgoing channels. Thus, the hypernuclear production cross section is expressed as a product of the cross section of the elementary cascade production reaction and a term that accounts for the dynamics of the relative motion. None of these models has attempted to calculate the cross sections of the elementary reaction - they have been extracted from the sparse experimental data. Therefore, the results of these calculations carry over the ambiguities that are involved in the experimental values of the differential cross sections for the elementary reactions.

In this paper, we investigate the production of cascade hypernuclei via the (K^-, K^+) reaction on nuclear targets within an effective Lagrangian model [32, 33, 34], which is similar to that used in Ref. [27] to study the elementary production reaction, $p(K^-, K^+)\Xi^-$. We consider only the s-channel production diagrams (see Fig. 1b) as we are interested in the region where p_{K^-} lies below 2 GeV/c. The model retains the full field theoretic structure of the interaction vertices and treats baryons as Dirac particles. The initial state interaction of the incoming K^- with a bound target proton leads to excitation of intermediate Λ and Σ resonant states, which propagate and subsequently decay into a Ξ^- hyperon that gets captured into one of the nuclear orbits, while the other decay product, the K^+ goes out. In Ref. [27], it was shown that six intermediate resonant states, Λ, $\Lambda(1405)$, $\Lambda(1520)$, $\Lambda(1810)$, Σ, and $\Sigma(1385)$, make the most significant contributions to the cross sections of the elementary process. Therefore, in our present study the amplitudes corresponding to these six resonant states have been considered.

2. Formalism

2.1. bound state spinors

The Ξ^- bound state spinors have been calculated in the quark-meson coupling (QMC) model as well as in a phenomenological model where they are obtained by solving the Dirac equation with scalar and vector fields having a Woods-Saxon (WS) radial form. In the latter case, with a set of radius and

Table 1: Parameters of the Dirac single particle potential (having a WS radial shape) for the Ξ^- bound and proton hole states. In each case radius (r_0) and diffuseness (a) parameters were 0.983 fm, and 0.606 fm, respectively for both vector and scalar potentials. The binding energies (BEs) of the Ξ^- states were taken from the predictions of the QMC model. The QMC BEs for the proton hole states are also shown together with the corresponding experimental values (given within the brackets).

State	BE (MeV)	V_v (MeV)	V_s (MeV)
${}^{12}_{\Xi^-}\mathrm{Be}(1s_{1/2})$	5.681	118.082	-145.780
${}^{28}_{\Xi^-}\mathrm{Mg}(1s_{1/2})$	11.376	124.674	-153.881
${}^{28}_{\Xi^-}\mathrm{Mg}(1p_{3/2})$	5.490	167.124	-206.326
${}^{28}_{\Xi^-}\mathrm{Mg}(1p_{1/2})$	5.836	181.486	-223.858
${}^{12}\mathrm{C}\ (1p_{3/2})$	14.329(15.957)	382.598	-472.343
${}^{28}\mathrm{Si}(1d_{5/2})$	10.071(11.585)	378.421	-467.186

diffuseness parameters, the depths of these fields are searched to reproduce the binding energy (BE) of a given state. Since the experimental values of the BEs for the Ξ^- bound states are as yet unknown, we have adopted the corresponding QMC model predictions (as shown in table 1) in our search procedure for these states. Furthermore, the scalar and vector fields are assumed to have the same geometry. It should be noted that the depths of the potential fields in such a model are dependent on the adopted radius (r_0) and diffuseness (a) parameters but there is no certain way of fixing them. Nevertheless, using same r_0 for all the states may make the search for the potential depths too restrictive. Some authors have used the root mean square radius (RMS) of a given state to fix the r_0 parameter (see, e.g., Refs. [35] and [36]). However, such a procedure cannot be applied for the Ξ bound states at this stage due to the lack of any experimental information about them. With these constraints, we show in Table 1 the resulting parameters associated with the scalar and vector fields of the phenomenological model for Ξ^- bound and proton hole states for the two target nuclei. In this table the QMC predictions for the BE of the proton hole states are also shown. However, in the search procedure for these states the experimental values of the BEs (given within the brackets) have been used.

The use of bound state spinors calculated within the QMC model provides an opportunity to investigate the role of the quark degrees of freedom in the cascade hypernuclear production, which has not been done in previous studies of this system. Since the cascade hypernuclear production involves large momentum transfers (350 MeV/c - 600 MeV/c) to the target nucleus, it is a good case for examining such short distance effects. In the QMC model [37], quarks within the non-overlapping nucleon bags (modeled using the MIT bag), interact self consistently with isoscalar-scalar (σ) and isoscalar-vector (ω) mesons in the mean field approximation. The explicit treatment of the nucleon internal structure represents an important departure from quantum hadrodynamics (QHD) model [38]. The self-consistent response of the bound quarks to the mean σ field leads to a new saturation mechanism for nuclear matter [37]. The QMC

model has been used to study the properties of finite nuclei [39], the binding of ω, η, η' and D nuclei [40, 41, 42] and also the effect of the medium on $K^{\pm}$ and J/Ψ production [43].

The most recent development of the quark-meson coupling model is the inclusion of the self-consistent effect of the mean scalar field on the familiar one-gluon exchange hyperfine interaction that in free space leads to the $N-\Delta$ and $\Sigma-\Lambda$ mass splitting [44]. With this [45] the QMC model has been able to explain the properties of Λ hypernuclei for the s-states rather well, while the p- and d-states tend to underbind. It also leads to a very natural explanation of the small spin-orbit force in Λ-nucleus interaction. In this exploratory work, the bound Ξ spinors are generated from this version of the QMC model and are used to calculate the cross sections of the $^{12}\mathrm{C}(K^-,K^+)^{12}_{\Xi^-}\mathrm{Be}$ and $^{28}\mathrm{Si}(K^-,K^+)^{28}_{\Xi^-}\mathrm{Mg}$ reactions.

To calculate the bound state spinors, we have used the latest version of the QMC model. In this version, while the quality of results for Λ and Ξ is comparable that of the earlier QMC results [41], no bound states for the Σ states [45] are found. The latter is in agreement with the experimental observations. This is facilitated by the extra repulsion associated with the increased one-gluon-exchange hyperfine interaction in medium. We refer to Ref. [45] for more details of this new version of the QMC.

In order to calculate the properties of finite hypernuclei, we construct a simple, relativistic shell model, with the nucleon core calculated in a combination of self-consistent scalar and vector mean fields. The Lagrangian density for a hypernuclear system in the QMC model is written as a sum of two terms, $\mathcal{L}^{HY}_{QMC} = \mathcal{L}_{QMC} + \mathcal{L}^{Y}_{QMC}$, where [40],

$$\begin{aligned}\mathcal{L}_{QMC} = \bar{\psi}_N(\boldsymbol{r})[i\gamma\cdot\partial - M_N(\sigma) - (\, g_\omega\omega(\boldsymbol{r}) \\ +g_\rho\frac{\tau_3^N}{2}b(\boldsymbol{r}) + \frac{e}{2}(1+\tau_3^N)A(\boldsymbol{r})\,)\gamma_0]\psi_N(\boldsymbol{r}) \\ -\frac{1}{2}[(\nabla\sigma(\boldsymbol{r}))^2 + m_\sigma^2\sigma(\boldsymbol{r})^2] \\ +\frac{1}{2}[(\nabla\omega(\boldsymbol{r}))^2 + m_\omega^2\omega(\boldsymbol{r})^2] \\ +\frac{1}{2}[(\nabla b(\boldsymbol{r}))^2 + m_\rho^2 b(\boldsymbol{r})^2] + \frac{1}{2}(\nabla A(\boldsymbol{r}))^2, \end{aligned} \tag{1}$$

and

$$\begin{aligned}\mathcal{L}^{Y}_{QMC} = \sum_{Y=\Lambda,\Sigma,\Xi}\overline{\psi}_Y(\boldsymbol{r})[i\gamma\cdot\partial - M_Y(\sigma) - (\, g^Y_\omega\omega(\boldsymbol{r}) \\ +g^Y_\rho I^Y_3 b(\boldsymbol{r}) + eQ_Y A(\boldsymbol{r})\,)\gamma_0]\psi_Y(\boldsymbol{r}), \end{aligned} \tag{2}$$

where $\psi_N(\boldsymbol{r})$, $\psi_Y(\boldsymbol{r})$, $b(\boldsymbol{r})$ and $\omega(r)$ are, respectively, the nucleon, hyperon, the ρ meson and the ω meson fields, while m_σ, m_ω and m_ρ are the masses of the σ, ω and ρ mesons. The $A(r)$ is Coulomb field. g_ω and g_ρ are the ω-N and ρ-N coupling constants which are related to the corresponding (u,d)-quark-ω, g^q_ω,

and (u,d) quark-ρ, g^q_ρ, coupling constants as $g_\omega = 3g^q_\omega$ and $g_\rho = g^q_\rho$. I^Y_3 and Q_Y are the third component of the hyperon isospin operator and its electric charge in units of the proton charge, e, respectively.

The following set of equations of motion are obtained for the hypernuclear system from the Lagrangian density Eqs. (1)-(2):

$$[i\gamma\cdot\partial - M_N(\sigma) - (\, g_\omega\omega(\boldsymbol{r}) + g_\rho\frac{\tau^N_3}{2}b(\boldsymbol{r}) + \frac{e}{2}(1+\tau^N_3)A(\boldsymbol{r})\,)\gamma_0]\psi_N(\boldsymbol{r}) = 0, \tag{3}$$

$$[i\gamma\cdot\partial - M_Y(\sigma) - (\, g^Y_\omega\omega(\boldsymbol{r}) + g_\rho I^Y_3 b(\boldsymbol{r}) + eQ_Y A(\boldsymbol{r})\,)\gamma_0]\psi_Y(\boldsymbol{r}) = 0, \tag{4}$$

$$(-\nabla^2_r + m^2_\sigma)\sigma(\boldsymbol{r}) = g_\sigma C_N(\sigma)\rho_s(\boldsymbol{r}) + g^Y_\sigma C_Y(\sigma)\rho^Y_s(\boldsymbol{r}), \tag{5}$$

$$(-\nabla^2_r + m^2_\omega)\omega(\boldsymbol{r}) = g_\omega\rho_B(\boldsymbol{r}) + g^Y_\omega\rho^Y_B(\boldsymbol{r}), \tag{6}$$

$$(-\nabla^2_r + m^2_\rho)b(\boldsymbol{r}) = \frac{g_\rho}{2}\rho_3(\boldsymbol{r}) + g^Y_\rho I^Y_3\rho^Y_B(\boldsymbol{r}), \tag{7}$$

$$(-\nabla^2_r)A(\boldsymbol{r}) = e\rho_p(\boldsymbol{r}) + eQ_Y\rho^Y_B(\boldsymbol{r}), \tag{8}$$

where, $\rho_s(\boldsymbol{r})$ $(\rho^Y_s(\boldsymbol{r}))$, $\rho_B(\boldsymbol{r})$ $(\rho^Y_B(\boldsymbol{r}))$, $\rho_3(\boldsymbol{r})$ and $\rho_p(\boldsymbol{r})$ are the scalar, baryon, third component of isovector, and proton densities at the position $\boldsymbol{r}$ in the hypernucleus [40]. On the right hand side of Eq. (5), a new and characteristic feature of QMC appears, arising from the internal structure of the nucleon and hyperon, namely, $g_\sigma C_N(\sigma) = -\frac{\partial M_N(\sigma)}{\partial\sigma}$ and $g^Y_\sigma C_Y(\sigma) = -\frac{\partial M_Y(\sigma)}{\partial\sigma}$ where $g_\sigma \equiv g_\sigma(\sigma=0)$ and $g^Y_\sigma \equiv g^Y_\sigma(\sigma=0)$. We use the nucleon and hyperon masses as parameterized in Ref. [45]. The scalar and vector fields as well as the spinors for hyperons and nucleons, can be obtained by solving these coupled equations self-consistently.

In Figs. 2(a) and Figs 2(c), we compare the scalar and vector fields as calculated within the QMC model with those of the phenomenological model for $1s_{1/2}$ Ξ^- states of ${}^{12}_{\Xi^-}$Be and ${}^{28}_{\Xi^-}$Mg hypernuclei, respectively. It may be recalled that in the QMC model the scalar and vector fields are generated by the couplings of the σ and ω mesons to the quarks. Because of the different masses of these mesons and their couplings to the quark fields the scalar and vector fields acquire a different radial dependence. In contrast, the two fields have the same radial shapes in the phenomenological model. We notice that in general, the QMC scalar and vector fields are smaller in magnitude than those of the phenomenological model in the entire r-region. One interesting point to note is

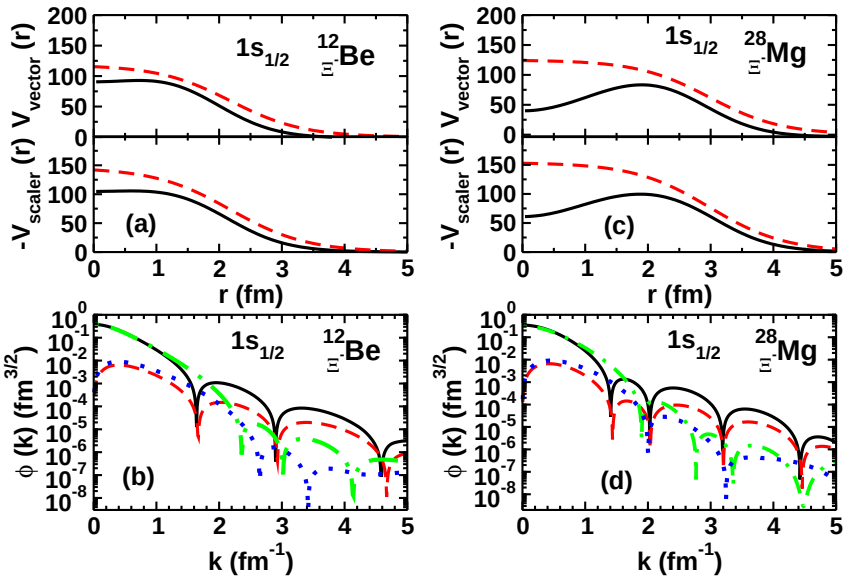

Figure 2: (color online) [(a)] Vector and scalar potential fields for $1s_{1/2}$ Ξ state in $^{12}_{\Xi^-}$Be. The QMC model and Dirac single particle results are shown by solid and dashed lines, respectively. [(b)] Moduli of the upper ($|f|$) and lower ($|g|$) components of the $1s_{1/2}$ Ξ orbits in $^{12}_{\Xi^-}$B hypernucleus in momentum space. $|f|$ and $|g|$ of the QMC model are shown by the solid and dashed lines, respectively while those of the phenomenological model by the dashed-dotted and dotted lines, respectively. [(c)] and [d] represent the same for $^{28}_{\Xi^-}$Mg hypernucleus.

that for the heavier hypernucleus, both scalar and vector QMC fields have their maxima away from the point $r = 0$, in contrast to the phenomenological fields. In the mean field models of the finite nuclei the proton densities are somewhat pushed out as compared to those of the neutron, because of Coulomb repulsion. This causes the Ξ^- potential to peak outside the center of the nucleus. This is a consequence of the self consistent procedure. In the case of a chargeless hyperon (e.g. Λ) such effects are not observed.

In Figs. 2(b) and 2(d) the moduli of the upper and lower components of $1s_{1/2}$ Ξ^- momentum space QMC (solid and dashed line) and phenomenological (dashed-dotted and dotted) spinors are shown for the $^{12}_{\Xi^-}$Be and $^{28}_{\Xi^-}$Mg hypernuclei, respectively. It is seen that the spinors of the two models are similar to each other for momenta (k) up to 2.0 fm^{-1}. Beyond this region, however, they start having differences. The position of minima in the phenomenological model spinors is shifted to higher values of k and their magnitudes are smaller than those of the QMC model. It should however, be remarked here that the structure of the minima reflects the size of the system. An improved search for the depths of the WS potentials in the phenomenological model as discussed, above might remove the differences seen between the spinors of the two models. We further note that only for k values below 1.5 fm^{-1}, are the magnitudes of the lower components, $|g(k)|$, substantially smaller than those of the upper

components. In the region of k pertinent to the cascade hypernuclear production, $|g(k)|$ may not be negligible. Thus the relativistic effects resulting from the small component of bound states spinors could be large for the hypernuclear production reactions on nuclei (see also the discussions presented in Ref. [46]).

2.2. Cross Sections for Hypernuclear Production

In order to calculate the amplitudes (and hence the cross sections) of the hypernuclear production reaction (see Fig. 1b), one requires the effective Lagrangians at the meson-baryon-resonance vertices and the corresponding coupling constants, and also the propagators for various resonances. After having established these quantities the amplitudes of the graphs of the type shown in Fig. 1 can be written by following the well known Feynman diagrams and can be computed numerically.

The effective Lagrangians for the resonance-kaon-baryon vertices for spin-$\frac{1}{2}$ and spin-$\frac{3}{2}$ resonances are taken as

$$\mathcal{L}_{KBR_{1/2}} = -g_{KBR_{1/2}}\bar{\psi}_{R_{1/2}}[\chi\, i\Gamma\,\varphi_K + \frac{(1-\chi)}{M}\,\Gamma\,\gamma_\mu\,(\partial^\mu\varphi_K)]\psi_B, \quad (9)$$

$$\mathcal{L}_{KBR_{3/2}} = \frac{g_{KBR_{3/2}}}{m_K}\bar{\psi}^\mu_{R_{3/2}}\partial_\mu\phi_K\psi_B + \text{h. c.}, \quad (10)$$

with $M = (m_R \pm m_B)$, where the upper sign corresponds to an even-parity and the lower sign to an odd-parity resonance, and B represents either a nucleon or a Ξ hyperon. The operator Γ is γ_5 (1) for an even- (odd-) parity resonance. The parameter χ controls the admixture of pseudoscalar and pseudovector components. The value of this parameter is taken to be 0.5 for the Λ^* and Σ^* states, but zero for Λ and Σ states, implying pure pseudovector couplings for the corresponding vertices in agreement with Refs. [33, 47]. It may be noted that the Lagrangian for spin-$\frac{3}{2}$ as given by Eq. (10) corresponds to that of a pure Rarita-Swinger form which has been used in all previous calculations of the hypernuclear production reactions within a similar effective Lagrangian model [32, 33, 34].

Similar to Ref. [27], we have used the following form factor at various vertices,

$$F_m(s) = \frac{\lambda^4}{\lambda^4 + (s-m^2)^2}, \quad (11)$$

where m is the mass of the propagating particle and λ is the cutoff parameter, which is taken to be 1.2 GeV everywhere which is the same as that used in Ref. [27].

The parameters of the resonance vertices were fixed in Ref. [27] by describing the total cross section data on elementary reactions $p(K^-, K^+)\Xi^-$ and $p(K^-, K^0)\Xi^0$, where the form of the spin-$\frac{3}{2}$ interaction vertex was somewhat different form that given Eq. (10). In this paper, therefore, we recalculate the cross sections of the elementary reaction using the spin-$\frac{3}{2}$ Lagrangian given by Eq. (10). Apart from the total cross sections, we also describe the differential cross sections of the $p(K^-, K^+)\Xi^-$ reaction which was not done in Ref. [27].

Table 2: Λ and Σ resonance intermediate states included in the calculations.

Intermediate state (R)	L_{I2J}	M (GeV)	$Width$ (GeV)	g_{KRN}	$g_{KR\Xi}$
Λ		1.116	0.0	-16.750	10.132
Σ		1.189	0.0	5.580	-13.50
$\Sigma(1385)$	P_{13}	1.383	0.036	-8.22	-8.220
$\Lambda(1405)$	S_{01}	1.406	0.050	1.585	-0.956
$\Lambda(1520)$	D_{03}	1.520	0.016	27.46	-16.610
$\Lambda(1810)$	P_{01}	1.810	0.150	2.800	2.800

The values of the vertex parameters were taken to be the same as those determined in Ref. [27] except for the vertices involving the $\Sigma(1385)$ resonance, where the coupling constants (CCs) have been slightly increased in order to better describe the differential cross section data (see Table 2).

The two interaction vertices of Fig. 1 are connected by a resonance propagator. For the spin-1/2 and spin-3/2 resonances the propagators are given by

$$\mathcal{D}_{R_{1/2}} = \frac{\mathrm{i}(\gamma_\mu p^\mu + m_{R_{1/2}})}{p^2 - (m_{R_{1/2}} - \mathrm{i}\Gamma_{R_{1/2}}/2)^2}, \tag{12}$$

and

$$\mathcal{D}^{\mu\nu}_{R_{3/2}} = -\frac{\mathrm{i}(\gamma_\lambda p^\lambda + m_{R_{3/2}})}{p^2 - (m_{R_{3/2}} - \mathrm{i}\Gamma_{R_{3/2}}/2)^2} P^{\mu\nu} \ , \tag{13}$$

respectively. In Eq. (13) we have defined

$$P^{\mu\nu} = g^{\mu\nu} - \frac{1}{3}\gamma^\mu\gamma^\nu - \frac{2}{3m^2_{R_{3/2}}} p^\mu p^\nu + \frac{1}{3m_{R_{3/2}}} \left(p^\mu\gamma^\nu - p^\nu\gamma^\mu\right) \ . \tag{14}$$

In Eqs. (12) and (13), $\Gamma_{R_{1/2}}$ and $\Gamma_{R_{3/2}}$ define the total widths of the corresponding resonances. We have ignored any medium modification of the resonance widths while calculating the amplitudes of the hypernuclear production as information about them is scarce and uncertain.

In the next section we describe the results of our calculations for the (K^-, K^+) reaction on both proton and nuclear targets.

3. Results and Discussions

In Figs. 3a, we show comparisons of our calculations with the data for the total cross section of the $p(K^-, K^+)\Xi^-$ reaction for K^- beam momenta (p_{K^-}) below 3.5 GeV/c, because the resonance picture is not suitable at momenta higher than this. It is clear that our model is able to describe well the beam momentum dependence of the total cross section data of the elementary reactions within statistical errors. The arrow in Fig. 3a shows the position of the

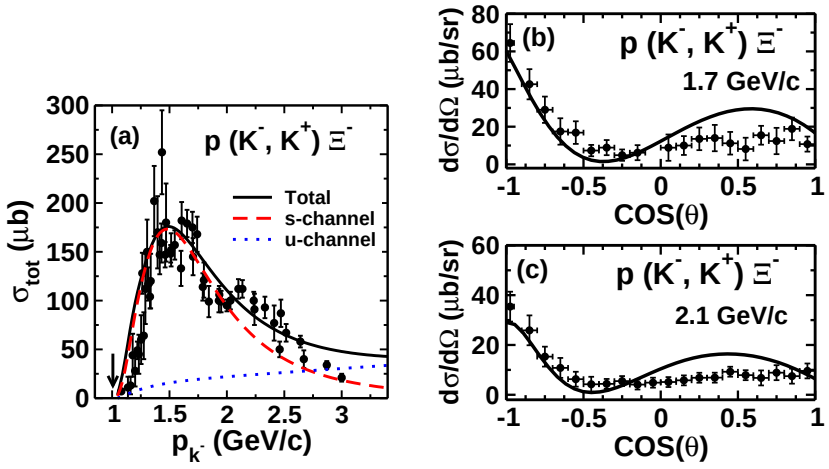

Figure 3: (color online) (a) Comparison of the calculated total cross section for the $p(K^-, K^+)\Xi^-$ reaction as a function of incident K^- momentum with the corresponding experimental data. Also shown are the individual contributions of s- and u-channel diagrams to the total cross section. The arrow indicates the position of the threshold for this reaction. (b) and (c) Differential cross sections for the same reaction for K^- beam momenta of 1.7 GeV/c and 2.1 GeV/c, respectively.

threshold beam momentum for this reaction which is about 1.0 GeV. The measured total cross section peaks in the region of 1.35-1.4 GeV/c which is well described by our model. We further note that the cross sections for $p_{K^-} < 2.0$ GeV/c are dominated by the s-channel contributions.

In Fig. 3b we compare our calculations with the differential cross section data of the $p(K^-, K^+)\Xi^-$ reaction for p_{K^-} values of 1.7 GeV/c and 2.1 GeV/c. These data were read from the corresponding figures given in Ref. [24]. Both calculated and experimental differential cross sections are normalized to the same total cross section. We see that our calculations describe the general trends of the angular distribution data well in the entire angular region for both the beam momenta. Nevertheless, a slight overestimate of the data is noted at the forward angles. There is a need to remeasure these differential cross sections at the JPARC facility to confirm and refine the old bubble chamber data of Ref. [24].

The beam momentum dependence of the 0° differential cross section $(d\sigma/d\Omega)_{0^\circ}$ for the $p(K^-, K^+)\Xi^-$ reaction is an interesting quantity because it enters explicitly into the expression for the cross sections of the (K^-, K^+) reaction on nuclei (leading to the production of Ξ hypernuclei) in the kind of model used in Ref. [19]. Hence, the beam energy dependence of the zero angle differential cross section of the hypernuclear production directly follows that of $[(d\sigma/d\Omega)_{0^\circ}]$. In Fig. 4, we show the beam momentum dependence of this quantity (using the same normalization as those in Figs. 3b and 3c). We see that $[(d\sigma/d\Omega)_{0^\circ}]$ peaks in the same region of p_{K^-} as the total cross section shown in Fig. 3a. On the other hand, the situation regarding the momentum dependence of the available

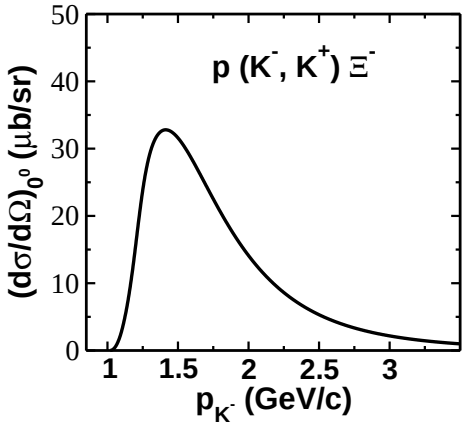

Figure 4: (color online) The zero degree differential cross section of the $p(K^-, K^+)\Xi^-$ reaction calculated as a function of beam momentum.

experimental data on $[(d\sigma/d\Omega)_{0^\circ}]$ is quite uncertain. The existing data reported in Refs. [21, 23, 24] differ considerably from each other. This may be due to normalization problems between different experiments or may be arising from the large errors in the Legendre coefficients. In fact only Ref. [24] shows the data explicitly for four values of p_{K^-} between 1.7 GeV/c to 2.64 GeV/c, together with the coefficients of the Legendre polynomial fits to the data. The other two references give only the coefficients of such a fit that have large correlated errors. The cross sections of Ref. [21] could have maxima at both 1.4 GeV/c and 1.7 GeV/c within the statistical errors. The data of Ref. [23] have a peak at 1.74 GeV/c but the coefficients of the Legendre polynomial fits given there may have misprints - at one beam momentum they even give negative cross section. Therefore, the position of the peak in the experimental zero degree differential cross section of the $p(K^-, K^+)\Xi^-$ is uncertain. A proper measurement of this quantity at the JPARC facility would be very welcome in order to remove this anomaly.

In calculations of the hypernuclear production reactions, we have employed pure single-particle-single-hole (Ξp^{-1}) wave functions to describe the nuclear structure part, ignoring any configuration mixing effects. The nuclear structure part is treated exactly in the same way as described in Ref. [33]. The amplitude involves the momentum space four component (spin space) spinors (ψ) which represent the wave functions of the bound states of nucleon and hyperon. For the proton hole and Ξ^- states, spinors generated within the QMC and the phenomenological models were used in the respective calculations. We have used a plane wave approximation to describe the relative motion of kaons in the incoming and outgoing channels. However, the distortion effects are partially accounted for by introducing reduction factors to the cross sections as described in Ref. [29]. Since our calculations are carried out all along in momentum space, they include all the nonlocalities in the production amplitudes that arise from

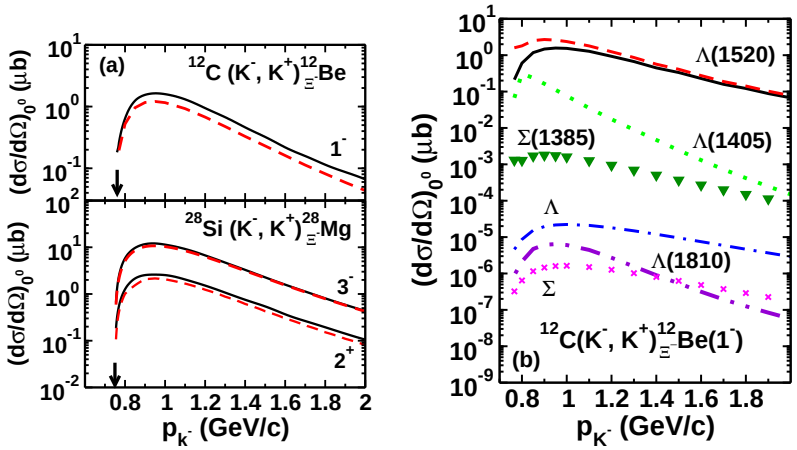

Figure 5: (color online) (a) Calculated differential cross section at 0° as a function of K^- beam momentum for the ^{12}C$(K^-, K^+)^{12}_{\Xi^-}$Be and ^{28}Si$(K^-, K^+)^{28}_{\Xi^-}$Mg reactions. The spin-parity of the final hypernuclear states are indicated on each curve. The particle-hole configurations of the $^{12}_{\Xi^-}$Be(1^-) and the $^{28}_{\Xi^-}$Mg(2^+) hypernuclear states are $[(1p_{3/2})_p^{-1}, (1s_{1/2})_{\Xi^-}]1^-$, and $[(1d_{5/2})_p^{-1}, (1s_{1/2})_{\Xi^-}]2^+$, respectively. For the $^{28}_{\Xi^-}$Mg(3^-) state the results shown are the sum of the cross section corresponding to both $[(1d_{5/2})_p^{-1}, (1p_{3/2})_{\Xi^-}]3^-$ and $[(1d_{5/2})_p^{-1}, (1p_{1/2})_{\Xi^-}]3^-$ configurations. The solid and dashed lines represent the results obtained with the QMC and the phenomenological Ξ^- bound state spinors. Arrows show the threshold of the two reactions. (b) Contributions of individual resonance intermediate states as indicated near each line, to the zero angle differential cross section as function of K^- beam momentum for the ^{12}C$(K^-, K^+)^{12}_{\Xi^-}$Be(1^-) reaction. Their coherent sum is shown by the solid line.

the resonance propagators.

We have chosen the reactions ^{12}C$(K^-, K^+)^{12}_{\Xi^-}$Be and ^{28}Si$(K^-, K^+)^{28}_{\Xi^-}$Mg for the first application of our model. The reaction on the ^{12}C target is billed as the "day one" experiment at the JPARC facility. The thresholds for these reactions are about 0.761 GeV/c and 0.750 GeV/c, respectively and the momentum transfers involved at 0°, vary between 1.8 - 2.9 fm^{-1}. The initial states in both the cases are doubly closed systems. The QMC model predicts only one bound state for the $^{12}_{\Xi^-}$Be hypernucleus with the Ξ^- hyperon being in a $1s_{1/2}$ state with a binding energy as shown in Table 1. For the $^{28}_{\Xi^-}$Mg case however, three distinct bound Ξ^- states with configurations $1s_{1/2}$, $1p_{3/2}$ and $1p_{1/2}$ have been predicted. The binding energies of these states are shown in Table 1. It is evident that for this nucleus $1p_{3/2}$ and $1p_{1/2}$ states are almost degenerate. This reflects the fact that the Ξ-nucleus spin-orbit potential is weak. This is due to the fact that since the corresponding total potential depth is small, the gradient of this potential that contributes to the spin-orbit force is also small.

In case of the ^{12}C target, the Ξ^- hyperon in a $1s_{1/2}$ state can populate 1^- and 2^- states of the hypernucleus corresponding to the particle-hole configuration $[(1p_{3/2})_p^{-1}, (1s_{1/2})_{\Xi^-}]$. The states populated for the $^{28}_{\Xi^-}$Mg hypernucleus are $[2^+, 3^+]$, $[1^-, 2^-, 3^-, 4^-]$, and $[2^-, 3^-]$ corresponding to the configura-

tions $[(1d_{5/2})_p^{-1}, (1s_{1/2})_{\Xi^-}]$, $[(1d_{5/2})_p^{-1}, (1p_{3/2})_{\Xi^-}]$, and $[(1d_{5/2})_p^{-1}, (1p_{1/2})_{\Xi^-}]$, respectively. In Fig. 5, we have shown results for populating the hypernuclear state with maximum spin of natural parity for each configuration. The unnatural parity states are very weakly excited due to the vanishingly small spin-flip amplitudes for this reaction (see, e.g., Ref. [19] for an extensive discussion on this point). However, for the ${}^{28}_{\Xi^-}\mathrm{Mg}(3^-)$ case, the results shown are the sum of the cross sections obtained with both $[(1d_{5/2})_p^{-1}, (1p_{3/2})_{\Xi^-}]$ and $[(1d_{5/2})_p^{-1}, (1p_{1/2})_{\Xi^-}]$ particle-hole configurations. The latter contributes substantially (up to about 75% within our model) to the excitation of this state.

In Fig. 5a, the 0° differential cross sections are shown as a function of the beam momentum that are obtained by using Ξ^- bound state spinors calculated within the QMC as well as the phenomenological model for the reactions ${}^{12}\mathrm{C}(K^-, K^+){}^{12}_{\Xi^-}\mathrm{Be}$ and ${}^{28}\mathrm{Si}(K^-, K^+){}^{28}_{\Xi^-}\mathrm{Mg}$. The configurations of the final hypernuclear states are as described in the figure caption. In the calculations of our reaction amplitudes, the relative motions of K^- and K^+ mesons in the initial and final channels, respectively are described by plane waves. The distortion effects, which primarily describe the absorption of the incoming K^-, are however, included by introducing factors that reduce the magnitudes of the cross sections. These factors are taken to be 2.8 and 5.0 for ${}^{12}\mathrm{C}$ and ${}^{28}\mathrm{Si}$ targets, respectively as suggested in Ref. [29]. This necessarily assumes that shapes of the angular distributions are not affected by the distortion effects. This aspect will be further investigated in a future study.

We see that the QMC model cross sections are larger than those obtained by using the phenomenological model by about 10-15% in all the cases. This reflects the fact that in the region of momentum transfers relevant to these reactions both the upper and the lower components of the QMC spinors are higher in magnitude than the corresponding phenomenological ones.

An important observation in Fig. 5a is that for both the hypernuclear production reactions, the cross sections peak at p_{K^-} around 1.0 GeV/c, which is about 0.25-0.26 GeV/c above the production thresholds of the two reactions. Interestingly, it is not too different from the case of the elementary Ξ^- production reaction where the peaks of the total cross section as well as the zero degree differential cross section occur at about 0.35-0.40 GeV/c above the corresponding production threshold (see Figa. 3a and 4). Furthermore, the magnitudes of the cross sections near the peak position are in excess of 1 μb. It is important in this context to note that the magnitude of our cross section for a ${}^{12}\mathrm{C}$ target at a beam momentum of 1.6 GeV/c is similar to that obtained in Ref. [29] within an impulse approximation model. Moreover, our cross sections at 1.8 GeV/c also are very close those of Ref. [19] for both the targets. However, we fail to corroborate the results of Ref. [19] where cross sections were shown to peak for p_{K^-} around 1.8 GeV/c. It is quite probable that the distortion effects are dependent on the beam momenta and may be relatively stronger at lower values of p_{K^-}. Nevertheless, this is unlikely to lead to such a large shift in the peak position. In any case, this effect was not considered in Ref. [19] also. There may be a need to re-examine the beam momentum dependence of the zero degree differential cross section in order to understand this different.

In Fig 5b, we note that the contribution from the $\Lambda(1520)$ intermediate state dominates the total cross sections over the entire regime of p_{K^-} values. This is similar to that noted in the case of the elementary Ξ^- production reaction. The $\Lambda(1405)$, and $\Sigma(1385)$ states make noticeable contributions only for p_{K^-} very close to the production threshold. Other resonances contribute very weakly. Of course, our results are quite dependent on the CCs of various vertices, which are somewhat uncertain. Nevertheless, the respective cross sections shown in this figure are robust. First of all these CCs provide a good description of the total as well a differential cross sections of the elementary Ξ^- production reaction. Secondly there is very little scope for increasing further the individual contributions of the Λ and Σ intermediate states, because the CCs of the corresponding vertices used by us are already larger than their upper limits suggested in the literature. Furthermore, the contributions of other resonances are too weak and even have the wrong p_{K^-} dependence. Therefore, the final results are unlikely to be affected too much by the known uncertainties in the corresponding CCs.

4. Summary and Conclusions

In summary, in this paper the cascade hypernuclear production reactions $^{12}\mathrm{C}(K^-,K^+)^{12}_{\Xi^-}\mathrm{Be}$, and $^{28}\mathrm{Si}(K^-,K^+)^{28}_{\Xi^-}\mathrm{Mg}$ have been studied within an effective Lagrangian model, using the proton hole and Ξ^- bound state spinors derived from the latest quark-meson coupling model. This is for the first time that the quark degrees of freedom have been explicitly invoked in the description of such reactions. We have considered the excitation of altogether six Λ and Σ hyperon resonance intermediate states in the initial collision of the K^- meson with a target proton. These states subsequently propagate and decay into a Ξ^- hyperon and a K^+ meson. The hyperon gets captured in one of the nuclear orbits, while the meson goes out. We constrain the coupling constants at the resonance vertices by describing both the total and the differential cross sections of the elementary $p(K^+,K^-)\Xi^-$ reaction within a similar model.

We have also performed calculations with the spinors obtained by solving the Dirac equation with vector and scalar potential fields having Woods-Saxon shapes (the phenomenological model). Their depths are fitted to the binding energies of the respective states (QMC model values for the Ξ^- particle states and experimental values for the proton hole states) for a given set of geometry parameters which are taken to be the same for the two fields. While for $^{12}_{\Xi^-}\mathrm{Be}$ hypernucleus the shapes of the QMC fields are similar to those of the phenomenological model, the two differ considerably in the case of $^{28}_{\Xi^-}\mathrm{Mg}$. For the cases studied in this paper, the hypernuclear production cross sections calculated with the QMC Ξ^- spinors are found to differ only slightly from those obtained within the phenomenological (the former being about 10-15% higher in magnitude than the later). The distortion effects are included by introducing reduction factors to the cross sections taken from the previous studies of this reaction.

The zero degree differential cross sections for the Ξ^- hypernuclear production reactions on the two targets considered here, have peaks around the beam

momentum of 1.0 GeV/c within both the QMC and the phenomenological models. This peak momentum is above the corresponding production threshold by almost the same amount as the position of the maximum in the elementary total as well as zero degree differential cross sections lies away from its respective threshold. The peak cross sections are in excess of 1 μb. Furthermore, the total hypernuclear production cross sections are dominated by the contributions from the $\Lambda(1520)$ (D_{03}) resonance intermediate state which is similar to the case of the elementary Ξ^- production reaction. Other resonances make noticeable contributions only at beam momenta close to the production threshold of the reaction. It is desirable to perform measurements for the differential cross sections of the elementary Ξ^- production reaction in a wide beam momentum range.

This work was supported by the University of Adelaide and the Australian Research Council through grant FL0992247(AWT).

Bibliography

[1] T. A. Rijken, M. M. Nagels and Y. Yamamoto, Progr. Theo. Phys. (supplement), 185 (2010) 14.

[2] J. Schaffner-Bielich, Nucl. Phys. **A 804** (2008) 309; *ibid.* Nucl. Phys. **A 835** (2010) 279c.

[3] J. M. Lattimer and M. Prakash, Science **304** (2004) 536.

[4] J. Adams *et al.*, Phys. Rev. Lett. **98** (2007) 062301; J. H. Chen, Nucl. Phys. **835** (2010) 117c.

[5] K. Aamodt *et al.* (ALICE collaboration), Phys. Rev. Lett. **106** (2011) 032301.

[6] CBM Physics Book, Springer, 2011; http://www.gsi.de/fair/experiment/CBM/PhysicsBook.html

[7] R. L. Jaffe, Phys. Rev. Lett. **38** (1977) 195

[8] P. J. Mulders and A. W. Thomas, J. Phys. G **9** (1983) 1159.

[9] S. R. Beane *et al.*, Phys. Rev. Lett. **106** (2011) 162001; T. Inoue *et al.*, *ibid.* **106** (2011) 162002; P. E. Shanahan, A. W. Thomas, and R. D. Young, *ibid.* (2011) 092004.

[10] A. T. M. Aerts and C. B. Dover, Phys. Rev. Lett. **49** (1982) 1752.

[11] A. T. M.Aerts and C. B.Dover, Phys. Rev. D **28** (1983) 450.

[12] T. Iijima it et al., Nucl. Phys. **A 546** (1992) 588.

[13] T. Fukuda *et al.*, Phys. Rev. C **58** (1998) 1306.

[14] J. K. Ahn *et al.*(KEK-PS E224 Collaboration), Phys. Lett. **B444** (1998) 267.

[15] P. Khaustov *et al.*, Phys. Rev. C **61** (2000) 054603.

[16] C. J. Yoon *et al.* (KEK-PS E522 Collaboration), Phys. Rev. C **75** (2007) 022201 (R).

[17] D. H. Wilkinson *et al.*, Phys. Rev. Lett. **3** (1959) 397; A. Bechdolff *et al.*, Phys. Lett. **B26** (1968) 174.

[18] T. Nagae *et al.*, JPARC proposal E05, http://j-parc.jp/NuclPart/Proposal_e.html.

[19] C. B. Dover and A. Gal, Ann. Phys. (NY) **146** (1983) 309.

[20] G. M. Pjerrou *et al.*, Phys. Rev. Lett. **9**, 114 (1962).

[21] J. Peter Berg *et al.*, Phys. Rev. **147**, 945 (1966).

[22] D. W. Merrill and J. Button-Shafer, *ibid.* **167**, 1202 (1968).

[23] G. Burgun *et al.*, Nucl. Phys. **B8**, 447 (1968).

[24] P. M. Dauber *et al.*, Phys. Rev. **179**, 1262 (1969).

[25] J. R. Carlson *et al.*, Phys. Rev. D **7**, 2533 (1973). E. Briefel *et al.*, Phys. Rev. D **16**, 2706 (1977).

[26] V. Flaminio *et al.* CERN-HERA Report No. 83-02, 1983.

[27] R. Shyam, O. Scholten and A. W. Thomas, Phys. Rev. C **84** (2011) 042201(R).

[28] Y. Yamamoto, T. Motoba, T. Fukuda, M. Takahashi and K. Ikeda, Progr. Theo. Phys. Suppl. **117** (1994) 281.

[29] K. Ikeda, T. Fukuda, T. Motoba, M. Takahashi and Y. Yamamoto, Progr. Theo. Phys. **91** (1994) 747.

[30] S. Tadokoro, H. Kobayashi, and Y. Akaishi, Phys. Rev. C **51** (1995) 2656.

[31] T. Harada, Y. Hirabayashi and A. Umeya, Phys. Lett. **B 690** (2010) 363.

[32] R. Shyam, H, Lenske and U. Mosel, Phys. Rev. C **69** (2004) 065205; *ibid.*, Nucl. Phys. **A764** (2006) 313.

[33] R. Shyam, H. Lenske and U. Mosel, Phys. Rev. C **77** (2008) 052201(R).

[34] R. Shyam, K. Tsushima and A. W. Thomas, Phys. Lett. **B676** (2009) 51.

[35] W. Peters, H. Lenske and U. Mosel, Nucl. Phys. **A640** (1998) 89.

[36] S. Bender, R. Shyam and H. Lenske, Nucl. Phys. **A 839** (2010) 51.

[37] P. A. M. Guichon, Phys. Lett. **B200** (1988) 235; P. A. M. Guichon, K. Saito, E. N. Rodionov, and A. W. Thomas, Nucl. Phys. **A601** (1996) 349; P. A. M. Guichon, H. H. Matevosyan, N. Sandulescu, A. W. Thomas, Nucl. Phys. **A772** (2006) 1; K. Saito and A. W. Thomas, Phys. Rev. C **51** (1995) 2757.

[38] B. D. Serot and J. D. Walecka, Adv. Nucl. Phys. **16** (1986) 1; *ibid*, Int. J. Mod. Phys. **E 6** (1997) 515.

[39] K. Saito, K. Tsushima and A. W. Thomas, Nucl. Phys. **A609** (1996) 339.

[40] K. Tsushima, D. H. Lu, A. W. Thomas, and K. Saito, Phys. Lett. B443 (1998) 26.

[41] K. Tsushima, K. Saito, J. Haidenbauer and A. W. Thomas, Nucl. Phys. **A630** (1998) 691.

[42] K. Tsushima, D. H. Lu, A. W. Thomas, K. Saito R. H. Landau, Phys. Rev. C **59** (1999) 2824; S. D. Bass and A. W. Thomas, Phys. Lett. B634 (2006) 368.

[43] K. Saito, K. Tsushima and A. W. Thomas, Prog. Part. Nucl. Phys. **58** (2007) 1.

[44] J. Rikovska-Stone, P. A. M. Guichon, H. H. Matevosyan and A. W. Thomas, Nucl. Phys. **A792** (2007) 341.

[45] P. A. M. Guichon, A. W. Thomas, and K. Tsushima, Nucl. Phys. **A 814** (2008) 66.

[46] C. Bennhold and L. E. Wright, Phys. Rev. C **39** (1989) 927; *ibid*, Phys. Lett. **B191** (1987) 11.

[47] R. Shyam, Phys. Rev. C **60** (1999) 055213.